

Catalyst-loaded Micro-encapsulated Phase Change Material for Thermal Control of Exothermic Reaction

Tatsuya Takahashi

Hokkaido University

Hiroaki Koide

Hokkaido University

Hiroki Sakai

Hokkaido University

Daisuke Ajito

Hokkaido University

Ade Kurniawan

Hokkaido University

Yuji Kunisada

Hokkaido University

Takahiro Nomura (✉ nms-tropy@eng.hokudai.ac.jp)

Hokkaido University

Research Article

Keywords: Thermal control, Phase change material, Microcapsule, CO₂ methanation, Catalyst. CCUS (Carbon dioxide Capture, Utilization and Storage)

Posted Date: December 10th, 2020

DOI: <https://doi.org/10.21203/rs.3.rs-122324/v1>

License:  This work is licensed under a Creative Commons Attribution 4.0 International License.

[Read Full License](#)

Version of Record: A version of this preprint was published at Scientific Reports on April 6th, 2021. See the published version at <https://doi.org/10.1038/s41598-021-86117-1>.

Title

**Catalyst-loaded micro-encapsulated phase change material
for thermal control of exothermic reaction**

Tatsuya Takahashi¹, Hiroaki Koide¹, Sakai Hiroki¹, Daisuke Ajito¹, Ade Kurniawan²,
and Yuji Kunisada², Takahiro Nomura^{2*}

¹*Graduate School of Engineering, Hokkaido University, Kita 13 Nishi 8, Kita-ku,
Sapporo, 060-8628 Japan*

²*Faculty of Engineering, Hokkaido University, Kita 13 Nishi 8, Kita-ku, Sapporo, 060-
8628 Japan*

**Corresponding author.*

Tel.: +81 11 706 6842; fax: +81 11 706 6849

E-mail address: nms-tropy@eng.hokudai.ac.jp (T.Nomura)

Abstract

CO₂ methanation is a promising technology to enable the use of CO₂ as a resource. Thermal control of CO₂ methanation, which is a highly active exothermic reaction, is important to avoid thermal runaway and subsequent degradation of the catalyst. Using the heat storage capacity of a phase change material (PCM) for thermal control of the reaction is a novel passive approach. In this study a novel structure was developed, wherein catalysts were directly loaded onto a micro-encapsulated PCM (MEPCM). The MEPCM was prepared in three steps consisting of a boehmite treatment, precipitation treatment, and heat oxidation treatment, and an impregnation process was adopted to prepare a Ni catalyst. The catalyst-loaded MEPCM did not show any breakage or deformation of the capsule or a decrease in the heat storage capacity after the impregnation treatment. MEPCM demonstrated a higher potential as an alternative catalyst support in CO₂ methanation than the commercially available α -Al₂O₃ particle. In addition, the heat storage capacity of the catalyst-loaded MEPCM suppressed the temperature rise of the catalyst bed at a high heat absorption rate (2.4 MW m⁻³). In conclusion, the catalyst-loaded MEPCM is a high-speed, high-precision thermal control device because of its high-density energy storage and resolution of a spatial gap between the catalyst and cooling devices. This novel concept has the potential to overcome the

technical challenges faced by efficiency enhancement of industrial chemical reactions.

Keywords

Thermal control; Phase change material; Microcapsule; CO₂ methanation; Catalyst; CCUS (Carbon dioxide Capture, Utilization and Storage)

1. Introduction

Thermal control is essential for operating various systems at appropriate temperatures and preventing system failures. Thermal runaway is one of the problems caused by an inability to properly control the reaction temperature. It is a positive loop state wherein the heat of an exothermic reaction causes the catalyst temperature to rise, which in turn promotes the reaction and further increases the catalyst temperature. This phenomenon occurs in chemical reactors and batteries and eventually results in the loss of control over the system and possible explosion¹⁻³. Thermal runaway in a heterogeneous catalytic reaction is also an economical problem because it reduces product selectivity, changes product distribution, and reduces the activity and life span of the catalyst². Industrial fixed-bed reactors are operated at relatively high temperatures for the efficient conversion of reactants to products¹. In this case, the temperature of the hot spot in the catalyst layer is close to the unstable range, and a slight disturbance in operating conditions can cause thermal runaway.

As one of the promising thermal control technologies, latent heat storage (LHS), which exploits the latent heat at the solid-liquid phase transformation of a phase change material (PCM), has attracted attention for its variety of positive characteristics, such as the release

and absorption of a large amount of heat within a small temperature range, high repeatability, and heat transfer at a constant temperature⁴⁻⁷. Therefore, LHS behaves as an isothermal heat sink when the operation temperature matches the melting temperature of the PCM and precise temperature control within a narrow range is expected. Furthermore, passive thermal control, including LHS, is used more often than active thermal control owing to its higher operational reliability and lower cost^{8,9}. However, the available temperature range of LHS depends mainly on the type of PCM used^{10,11}. Typically, molten salts or alloys are used in the high temperature range that favors a chemical reaction^{4,12,13}. Alloys are more promising than molten salts because of their high thermal conductivity, low volume expansion, and minimal supercooling^{12,13}. Some alloy PCMs have been reported recently. Blanco-Rodríguez et al. reported a Mg-Zn alloy, and Risueño et al. investigated Mg-Zn-Al alloys^{14,15}. In several of these studies, the leakage of molten PCM is a problem, and encapsulation of the PCM is essential to prevent it¹⁶.

Our research group previously developed a micro-encapsulated PCM (MEPCM) consisting of an Al-Si alloy core and an α -Al₂O₃ shell¹⁷⁻¹⁹. The MEPCM exhibited a high melting point above 500 °C, high heat storage density of 180 J g⁻¹ or higher, and durability over 3000 cycles. Furthermore, microscale encapsulation provided beneficial properties for thermal control: miniaturization of the PCM enabled rapid melting of the internal

alloy², and expansion of the heat exchange area provided rapid thermal response²⁰.

Several thermal control technologies utilizing LHS have been reported. Zhang et al. used In@SiO₂ capsules as a thermally functional additive to suppress the generation of local hot spots². Ademola et al. investigated a simulation of the Fischer-Tropsch reaction using PCM, wherein the reaction bed temperature was maintained in the appropriate range¹. LHS is also used to maintain the system temperature and to balance the heat demand and supply. Gokon et al. proposed a PCM-solar reactor to suppress the temperature change of a catalyst bed due to solar radiation fluctuation²¹; high catalyst performance was maintained for 30 min during the heat-discharging mode. Richard et al. proposed autothermal microchannel reactors in which the heat of the exothermic reaction was used in the endothermic reaction²². They confined the PCM layer between each reactor to suppress the thermal imbalance of the two reactions. On the other hand, when PCM is used as an additive in the catalyst layer or as a reactor jacket, the spatial gap between the heat source and PCM inhibits efficient heat conduction. Hence, the contact structure between the PCM surface and heat source is important for thermal control²³. Li et al. demonstrated the heat management of a chemical loop combustion in contact with Al@Al₂O₃ PCM microcapsules²³. However, there are few studies on thermal management components where a heat source was loaded onto the PCM

capsule.

Therefore, a structure in which the catalyst acts as a heat source for the exothermic reaction when loaded onto the surface of an MEPCM is a novel and promising heat control material. Ceramic materials, such as SiO₂, Al₂O₃, and TiO₂, are often used as catalyst supports due to their high heat resistance and chemical stability²⁴. Since the MEPCM shell consists of α -Al₂O₃, it can be used as a catalyst support. Fig. 1 shows a schematic diagram of the catalyst-loaded MEPCM and the thermal control system. The MEPCM, which is covered with fine particles of the catalyst, removes the heat generated on the catalyst surface during exothermic reactions at the nanoscale because of its heat storage capacity. Catalyst-loaded MEPCMs are used in combination with typical cooling devices (e.g., shell and tube reactor²⁵). These units cool the entire catalyst layer and prevent the PCM from losing its thermal storage characteristics due to a complete phase transformation. Thus, the catalyst-loaded MEPCM is expected to control the temperature of the entire catalyst layer at the nanoscale.

CO₂ methanation ($\text{CO}_2 + 4\text{H}_2 = \text{CH}_4 + 2\text{H}_2\text{O}(\text{g})$, $\Delta H_{298\text{K}}^0 = -164 \text{ kJ mol}^{-1}$) is considered as an important application of the catalyst-loaded MEPCM because of its demand for high thermal control²⁶. It presents an alternative to conventional natural gas production by converting CO₂ to CH₄, which is effective for reducing CO₂ emissions²⁷. Additionally,

CH₄ is superior to H₂ in terms of capital expenditure as transportation of CH₄ can be achieved by using existing natural gas pipelines^{27,28}. Based on the above, a power-to-gas system employing CO₂ methanation has been previously proposed^{25,29,30}. CO₂ methanation requires catalysts (Ni, Rh, Ru, etc.), and Ni, which is the most widely used, shows high catalytic activity from 300 to 400 °C^{28,31}. However, thermal runaway is a concern due to the highly exothermic reaction³²⁻³⁴. The use of a Ni-loaded MEPCM (Ni/MEPCM) instead of a conventional catalyst may suppress a significant rise in temperature.

The purpose of this study was to fabricate Ni/MEPCM and investigate its catalytic activity for CO₂ methanation and its thermal control characteristics during an exothermic reaction. Ni/MEPCM was fabricated by the conventional impregnation method because the MEPCM surface was assumed to behave in a manner similar to that of the surface of α -Al₂O₃ powder. A CO₂ methanation reaction was conducted to measure the catalytic performance. Based on the results, CO₂ conversion (%) and CH₄ selectivity (%) were estimated.

2. Methods

2. 1. Preparation of MEPCM

MEPCM was prepared from Al-Si microspheres (25 mass% Si; Diameter: < 38 μm , Purity: 99.0%, Hikari Material Industry Co. Ltd.). The melting point of the composition is approximately 577 $^{\circ}\text{C}$. The encapsulation of the microspheres was performed in three steps consisting of a boehmite treatment, precipitation treatment, and heat oxidation treatment, as proposed in a previous study¹⁹. First, 300 mL of distilled water containing 1.0 g of $\text{Al}(\text{OH})_3$ (Purity: 99.99%, Kojundo Chemical Lab. Co., Ltd.) was boiled with a hot stirrer. After adjusting the solution to a pH of 8.0 by adding a 1 M solution of NH_3 , 10 g of the Al-Si microspheres were added to the water. The mixture was continuously stirred for 3 h to form AlOOH shells on the surfaces of the microspheres by the hydration reaction. Second, the solutions were cooled to 75 $^{\circ}\text{C}$ and maintained at this temperature for 16 h. Subsequently, the precursor samples were filtered and dried at 105 $^{\circ}\text{C}$ overnight. Finally, 10 g of the precursor samples were heated from room temperature to 1150 $^{\circ}\text{C}$ at a rate of 10 $^{\circ}\text{C min}^{-1}$ and maintained there for 6 h under an O_2 gas flow (Purity: 99.5%, rate: 2.0 L min^{-1}) to form the $\alpha\text{-Al}_2\text{O}_3$ shells.

2. 2. Preparation of Ni/MEPCM

Ni loading onto the MEPCM was carried out by the impregnation method, here, the raw materials were adjusted so that the amount of nickel supported in the final product

was 10%. An aqueous solution containing 5.0 mL of distilled water and 0.50 g of $\text{Ni}(\text{NO}_3)_2 \cdot 6\text{H}_2\text{O}$ (Purity: 99.9%, Kojundo Chemical Lab. Co., Ltd.) was added to 0.90 g of the as-prepared MEPCM. The mixture was crystallized at 70 °C by a rotary evaporator (Shibata Scientific Technology Ltd, SRE-M3). The impregnated sample was dried at 105 °C for 24 h, then calcined at 500 °C for 4 h to prepare the Ni/MEPCM. Ni/ α - Al_2O_3 was also prepared for comparison by adding 0.90 g of α - Al_2O_3 (Diameter < 38 μm , Purity: 99.9%, Showa Denko Co., Ltd.) into another aqueous solution of distilled water and $\text{Ni}(\text{NO}_3)_2 \cdot 6\text{H}_2\text{O}$, as before, and the mixture was crystallized at 70 °C. The impregnated sample was then dried at 105 °C for 24 h and calcined at 500 °C for 4 h to prepare the Ni/ α - Al_2O_3 reference.

2. 3. Sample characterization

The phase compositions of the samples were characterized using X-ray powder diffraction (XRD, Rigaku, Miniflex600, Cu $K\alpha$). The morphology was observed by scanning electron microscopy-energy dispersive spectroscopy (SEM-EDS, JEOL, JSM-7400F). Brunauer–Emmett–Teller (BET) specific surface areas of the samples were analyzed based on the N_2 adsorption/desorption techniques using a gas adsorption analyzer (Yuasa Ionics, Autosorb 6AG). The density of the samples was measured using

a gas pycnometer (Quantachrome instruments, Ultrapycnometer1000). Additionally, the phase transition temperature and thermal storage ability were measured using a differential scanning calorimetry analyzer (DSC, Mettler-Toledo, TGA/DSC3+). The MEPCM sample was placed in an Al₂O₃ crucible and heated from room temperature to 600 °C at a rate of 2.0 °C min⁻¹ and maintained at this temperature for 5 min under an Ar gas flow (Purity 99.5%, rate 50 mL min⁻¹).

2. 4. CO₂ methanation

CO₂ methanation was performed in a vertical fixed bed tubular reactor (inner diameter: 6.0 mm) at atmospheric pressure to evaluate the catalytic activity tests. Fig. 2 shows a schematic diagram of the reactor. One-tenth of a gram of the samples were loaded into the reactor and fixed with quartz wool. The samples were reduced for 1 h at 500 °C under H₂ and Ar gas flow ($F_{in,H_2} = 40 \text{ mL min}^{-1}$ and $F_{in,Ar} = 100 \text{ mL min}^{-1}$, where $F_{in,x}$ represents the flow rate of the inlet gas). After cooling to the reaction temperature in Ar gas flow, the feed gas ($F_{in,CO_2} = 10 \text{ mL min}^{-1}$, $F_{in,H_2} = 40 \text{ mL min}^{-1}$, and $F_{in,Ar} = 110 \text{ mL min}^{-1}$) was introduced into the reactor for 1 h at 400 °C. The concentrations of the outlet gas was analyzed using a Quadrupole mass spectrometer (QMS, Pfeiffer Vacuum, Thermostar GSD301). CO₂ conversion and CH₄ selectivity were calculated using Eq. (1)

and (2):

$$\text{CO}_2 \text{ conversion (\%)} = \frac{(F_{\text{in, CO}_2} - F_{\text{out, CO}_2}) \times 100}{F_{\text{in, CO}_2}} \quad (1)$$

$$\text{CH}_4 \text{ selectivity (\%)} = \frac{F_{\text{out, CH}_4} \times 100}{(F_{\text{out, CH}_4} + F_{\text{out, CO}})} \quad (2)$$

where $F_{\text{out}, x}$ represents the flow rate of the outlet gas.

2. 5. Measurement of thermal control performance

The CO₂ methanation reaction was also used as a test to evaluate the thermal control characteristics of the Ni/MEPCM material. The reactions were carried out with Ni/MEPCM under two reaction conditions, and the temperature of the sample bed was measured in each case. The difference between the two conditions determined whether the internal PCM was a solid or liquid (i.e., whether the samples had a heat storage capacity or not). The temperature control performance of the PCM was evaluated from the difference between these temperatures.

The reaction was carried out in the same reactor as in section 2.4., and the thermocouple was inserted into the middle of the sample bed to measure the temperature of the sample. Two-tenths of a gram of the PCM samples were loaded into the reactor such that the tip of the thermocouple was sufficiently covered by the samples. Fig. 3 shows the two different reaction conditions. In condition A, when the temperature of the sample layer exceeded the melting point of the PCM by the reaction heat, the phase transformation of

PCM occurred, and heat storage began. In condition B, the PCM melted before the reaction started, and the liquid state was maintained even at the reaction temperature for supercooling. Therefore, heat storage did not occur during the reaction. H₂ and Ar gas ($F_{in, H_2} = 40 \text{ mL min}^{-1}$ and $F_{in, Ar} = 100 \text{ mL min}^{-1}$) flowed during the reduction, and the feed gas ($F_{in, CO_2} = 15 \text{ mL min}^{-1}$, $F_{in, H_2} = 60 \text{ mL min}^{-1}$, and $F_{in, Ar} = 50 \text{ mL min}^{-1}$) was introduced during the reaction.

3. Results and Discussion

3. 1. Catalyst characterization

3. 1. 1. Phase composition of samples

Fig. 4 shows the XRD patterns of the MEPCM, Ni/MEPCM, and Ni/ α -Al₂O₃ samples. Peaks of Al, α -Al₂O₃, and Si were detected in the results of the MEPCM and Ni/MEPCM, and peaks of NiO was observed in the Ni/MEPCM. Peaks corresponding to α -Al₂O₃ and NiO were detected in the Ni/ α -Al₂O₃.

The XRD peaks of Al and Si were attributed to the core alloy in the MEPCM; meanwhile, the α -Al₂O₃ peak was attributed to its shell. Stronger peaks of α -Al₂O₃ were observed in the Ni/ α -Al₂O₃ than in the other samples. This is due to the fact that only the shell of the MEPCM was composed of α -Al₂O₃ as opposed to the entire structure of Ni/ α -

Al₂O₃. Since the peaks of NiO and α -Al₂O₃ were similar in all samples, the prepared samples were expected to have similar catalytic properties.

3. 1. 2. Morphology of samples

Fig. 5 shows the SEM images and elemental mapping results of the MEPCM, Ni/MEPCM, and Ni/ α -Al₂O₃ samples. The entire surface of the MEPCM was covered with a needle-like structure, and cuboid crystals had formed on the structure. The same structure along with fine particles of approximately 40 nm in diameter were present in the Ni/MEPCM. A smooth surface was detected in the Ni/ α -Al₂O₃, and fine particles of approximately 100 nm in diameter were present on its surface. In the elemental mapping, the MEPCM shell was composed of Al, O, and a small amount of Si, while Ni was present on the MEPCM shell after Ni impregnation in the Ni/MEPCM. In contrast, Al, O, and Ni were strongly detected in the Ni/ α -Al₂O₃.

The needle-like structure and cuboid crystals were composed of Al and O, and the XRD patterns reveal α -Al₂O₃ peaks. Thus, the MEPCM shells had formed only from α -Al₂O₃. The characteristic needle-like structures corresponded to AlOOH formed during the boehmite treatment¹⁷. The cuboid crystals represented the deposited or adhered Al(OH)₃ particles formed during the precipitation treatment¹⁹. These two types of structures

created a coarse configuration. The small amount of Si that was detected implied that most of the Si was present only in the MEPCM core. The fine particles were present only in the Ni-impregnated sample; thus, they were considered to be NiO from the elemental mapping and XRD patterns. Ni was supported on the MEPCM without aggregation since these particles were distributed. As the core/shell structure was neither broken nor deformed, and there was no elemental mapping of Si outside the capsules, no apparent core leakage occurred during the impregnation process. On the other hand, in Ni/ α -Al₂O₃, the particles recognized as NiO were more aggregated than those in the Ni/MEPCM, and Si was determined as a trace impurity in the production.

3. 1. 3. BET specific surface area of samples

Table 1 shows the BET specific surface areas and densities of the MEPCM, Ni/MEPCM, and Ni/ α -Al₂O₃. A difference in the interior composition of the Ni/MEPCM and Ni/ α -Al₂O₃ caused a difference in mass even at equal volumes. Therefore, these samples should be evaluated by the BET specific surface area per volume, which was converted from the specific surface area per mass using the density of each sample. The Ni/MEPCM had the largest BET specific surface area at $38.2 \times 10^6 \text{ m}^2 \text{ m}^{-3}$.

Table 1 BET specific surface areas per mass or volume, and densities of the MEPCM, Ni/MEPCM, and Ni/ α -Al₂O₃.

	MEPCM	Ni/MEPCM	Ni/ α -Al ₂ O ₃
BET surface area (m ² g ⁻¹)	10.19	11.28	2.75
Density (g m ⁻³)	2.69×10 ⁶	3.39×10 ⁶	4.11×10 ⁶
BET surface area (m ² m ⁻³)	27.4×10 ⁶	38.2×10 ⁶	11.3×10 ⁶

The Ni/MEPCM showed a slightly larger surface area than that of the pure MEPCM since the crystals were formed on the surface of the MEPCM. At 11.3×10⁶ m² m⁻³, the surface area of the Ni/ α -Al₂O₃ was smaller than that of the MEPCM owing to the

smoother surface morphology of the α -Al₂O₃ particles. Generally, α -Al₂O₃ has a small specific surface area due to the formation process of α -Al₂O₃, whereby the high-temperature heat treatment facilitates the rearrangement of the Al₂O₃ particles and reduces the surface area³⁵. In contrast, the MEPCM had a higher specific surface area than that of ordinary α -Al₂O₃ powder because of its rough structure. Therefore, MEPCM is superior to α -Al₂O₃ powder as a catalyst support in terms of active-catalyst dispersion.

3. 2. Thermal properties

Fig. 6 shows the DSC curves during heating of the MEPCM, Ni/MEPCM, and Ni/ α -Al₂O₃ samples. An endothermic peak at approximately 573 °C is near the eutectic temperature of Al-Si alloy in both the MEPCM and Ni/MEPCM. Also, the LHS capacities of the MEPCM and Ni/MEPCM were different at 191.42 and 177.84 J g⁻¹, respectively. No endothermic peak was observed in the Ni/ α -Al₂O₃.

Since the onset temperature of the endothermic peak was close to the eutectic temperature (577 °C) of the Al-Si alloy, the endothermic peak arose from the phase change of the core alloy. Because Ni impregnated on the MEPCM as NiO particles (at 10 mass% Ni), the LHS capacity of the Ni/MEPCM was 202.47 J g⁻¹ if NiO was neglected. This value was not less than that of the MEPCM before Ni impregnation. Therefore, Ni

does not affect the heat storage capacity of the MEPCM.

3. 3. CO₂ methanation

The catalytic activity of each sample was evaluated by analyzing the outlet gas with a quadrupole mass spectrometer during CO₂ methanation. Fig. 7 shows the CO₂ conversion of each catalyst. The average CO₂ conversions of the Ni/MEPCM and Ni/ α -Al₂O₃ were 50% and 25%, respectively. In contrast, the value of the pure MEPCM was nearly 7%.

Since the pure MEPCM showed little catalytic activity, it was demonstrated that the Ni particles on the MEPCM drive catalytic activity. Moreover, the CO₂ conversion of the Ni/MEPCM exceeded that of the Ni/ α -Al₂O₃ by approximately 25%, suggesting that the MEPCM shell functions as a better catalyst support than ordinary α -Al₂O₃. This is attributed to the increase in the specific surface area of the MEPCM compared to that of the Ni/ α -Al₂O₃. Whereas the Ni loaded onto each sample showed the ability to promote CO₂ hydration, catalytic performances of Ni/MEPCM and Ni/ α -Al₂O₃ were poor because the theoretical equilibrium of CO₂ conversion was 97.50%, assuming only CH₄ and CO were generated at 400 °C³⁶.

Fig. 8 shows the CH₄ selectivity of each catalyst. The average CH₄ selectivity of the Ni/MEPCM and Ni/ α -Al₂O₃ were 62% and 40%, respectively. Meanwhile, the value of

the pure MEPCM could not be calculated because of the small amount of generated byproduct. Since the Ni/MEPCM possessed a higher CH₄ selectivity than Ni/ α -Al₂O₃, it is clear that the MEPCM can replace the α -Al₂O₃ support. The increase in the number of reaction sites was suspected as a factor for improving the CH₄ selectivity. This could be inferred from the following three points: (1) the CO₂ conversion of the Ni/MEPCM exceeded that of the Ni/ α -Al₂O₃; (2) the surface area of the Ni/MEPCM was larger than that of the Ni/ α -Al₂O₃; (3) SEM images showed aggregation of the NiO particles on the α -Al₂O₃.

CO₂ methanation on Ni generally passes through CO as an intermediate³⁷⁻³⁹; therefore, a certain extent of CO production may be caused by incomplete reactions. It is assumed that the CO generation decreased due to the completion of the reaction as a result of the increase in the number of reaction sites. In the future, a detailed investigation of the surface properties of the Ni/MEPCM is needed to support this discussion. Additionally, both CH₄ selectivities were lower than the theoretical equilibrium value, which is 99.87%, assuming only CH₄ and CO were generated at 400 °C³⁶.

3. 4. Thermal control performance

Fig. 9 shows the temperature change of the sample layer when CO₂ methanation was

performed under two conditions: with and without a heat storage capacity. These curves illustrate the average of five measurements, where feed gas was introduced 1 min after the measurement commenced. In both conditions, the temperature rose immediately after the injection of the feed gas. Without a heat storage capacity, the temperature of the sample layer increased linearly and stabilized at approximately 583 °C. When the sample had a heat storage capacity, the rising temperature trend behaved differently. The temperature of the sample layer rose linearly to approximately 573 °C, then gradually increased, stabilizing at approximately 583 °C. Each experiment showed the same reaction rates.

We considered that the final temperature stabilization was caused by the balance between the generated reaction heat and the heat lost to the outside of the reactor. A gradual temperature rise was observed only in the samples with a heat storage capacity. In addition, the gradual temperature rise started around 573 °C, which is close to eutectic temperature of the Al-Si alloy and the peak temperature of the phase transformation confirmed by DSC. Thus, we determined that the rate of increase of the temperature of the sample layer was lower because the thermal energy was expended on the phase change of the PCM (i.e., latent heat storage). It was confirmed that the catalyst-loaded MEPCM exhibited thermal control ability by slowing the rate of increase of the temperature of the

catalyst layer. The heat absorption rate of the Ni/MEPCM was calculated by Eq. (3).

$$W = \frac{Q_{0.2}}{\Delta t \times V} \quad (3)$$

In this formula, W (W m^{-3}) represents the heat absorption rate, $Q_{0.2}$ (J) and V (m^3) are the thermal storage capacity and volume, respectively, of 0.2 g of Ni/MEPCM, and Δt (s) is the time during which the Ni/MEPCM stored heat. In this study, the loaded sample volume was approximately $59 \times 10^{-9} \text{ m}^3$. The theoretical heat storage capacity of the loaded sample was approximately 171.7 J, as determined by DSC. Therefore, $Q_{0.2}$ was 34.3 J. Since the temperature difference between the two curves clearly occurred between 1 and 5 min, the PCM completed the phase transformation in 4 min ($\Delta t = 4 \text{ s}$). Therefore, the catalyst-loaded MEPCM exhibited an average rate of heat absorption of nearly 2.4 MW m^{-3} . In this calculation, the contribution of the sensible heat storage was neglected as the temperature difference between the two curves was insignificant. The resulting heat absorption rate is competitive with the heat exchange rate of some chemical heat storage materials and heat transfer technology that utilize LHS⁴⁰⁻⁴². This promising result comes from the fact that the MEPCM is a high-density energy storage device, and the novel structure of direct catalyst loading onto the PCM reduces the heat transfer distance.

4. Conclusion

The use of MEPCM as a catalyst support was explored to control the local temperature rise of catalyst layers. MEPCM was fabricated from Al-Si microspheres. Ni was introduced as a catalyst for the CO₂ methanation reaction by the impregnation method. The phase composition, morphology, and thermal storage capacity of the impregnated samples were evaluated. The catalyst performance of the Ni/MEPCM sample was investigated by estimating the CO₂ conversion and CH₄ selectivity when the CO₂ methanation reaction was performed at 400 °C. In addition, the thermal control characteristics of the MEPCM during an exothermic reaction were investigated. The primary results were as follows:

1) The phase composition, morphology, and heat storage capacity of the pure MEPCM did not change even after processing via the impregnation method. Nano-sized NiO particles were dispersed on the surface of the Ni/MEPCM. Therefore, the impregnation method, which is a conventional method for supporting catalysts, is applicable to MEPCM, and smooth scale-up can be expected for industrial applications.

2) The Ni/MEPCM exhibited appropriate performance as a catalyst support, with a significant increase in CO₂ conversion and CH₄ selectivity compared to those of α -Al₂O₃ particles.

3) Because of the heat storage capacity of Ni/MEPCM, it absorbed the reaction heat at a

favorable rate (2.4 MW m^{-3}) and reduced the rate of increase of the catalyst layer temperature during the exothermic reaction. The risk of thermal runaway may be reduced by combining the material with existing cooling techniques and optimizing the feed gas conditions.

In conclusion, MEPCM can be used as an alternative catalyst support due to the excellent stability and activity of its ceramic shell. In the future, the optimization of MEPCM as a catalyst support using surface modification will be pursued to realize higher efficiency in material conversion to improve the economical aspect of the technique.

- 1 Odunsi, A. O., O'Donovan, T. S. & Reay, D. A. Dynamic Modeling of Fixed-Bed Fischer-Tropsch Reactors with Phase Change Material Diluents. *Chemical Engineering &*

- Technology* **39**, 2066-2076, doi:10.1002/ceat.201600196 (2016).
- 2 Zhang, M. *et al.* Encapsulated nano-heat-sinks for thermal management of heterogeneous chemical reactions. *Nanoscale* **2**, doi:10.1039/c0nr00585a (2010).
- 3 Zhu, W. H. *et al.* A novel cooling structure with a matrix block of microfibrinous media / phase change materials for heat transfer enhancement in high power Li-ion battery packs. *Journal of Cleaner Production* **210**, 542-551, doi:10.1016/j.jclepro.2018.11.043 (2019).
- 4 Hasnain, S. M. Review on sustainable thermal energy storage technologies, part I: Heat storage materials and techniques. *Energy Convers. Manage.* **39**, 1127-1138, doi:Doi 10.1016/S0196-8904(98)00025-9 (1998).
- 5 Farid, M. M., Khudhair, A. M., Razack, S. A. K. & Al-Hallaj, S. A review on phase change energy storage: materials and applications. *Energy Convers. Manage.* **45**, 1597-1615, doi:10.1016/j.enconman.2003.09.015 (2004).
- 6 Nomura, T., Okinaka, N. & Akiyama, T. Technology of Latent Heat Storage for High Temperature Application: A Review. *ISIJ Int.* **50**, 1229-1239, doi:DOI 10.2355/isijinternational.50.1229 (2010).
- 7 Sharma, A., Tyagi, V. V., Chen, C. R. & Buddhi, D. Review on thermal energy storage with phase change materials and applications. *Renewable and Sustainable Energy Reviews* **13**, 318-345, doi:10.1016/j.rser.2007.10.005 (2009).
- 8 Xie, B., Cheng, W.-l. & Xu, Z.-m. Studies on the effect of shape-stabilized PCM filled aluminum honeycomb composite material on thermal control. *Int. J. Heat Mass Transfer* **91**, 135-143, doi:10.1016/j.ijheatmasstransfer.2015.07.108 (2015).
- 9 Sevinchan, E., Dincer, I. & Lang, H. A review on thermal management methods for robots. *Appl. Therm. Eng.* **140**, 799-813, doi:10.1016/j.applthermaleng.2018.04.132 (2018).
- 10 Jankowski, N. R. & McCluskey, F. P. A review of phase change materials for vehicle component thermal buffering. *Applied Energy* **113**, 1525-1561, doi:10.1016/j.apenergy.2013.08.026 (2014).
- 11 Peng, G., Dou, G., Hu, Y., Sun, Y. & Chen, Z. Phase Change Material (PCM) Microcapsules for Thermal Energy Storage. *Adv. Polym. Tech.* **2020**, 1-20, doi:10.1155/2020/9490873 (2020).
- 12 Kenisarin, M. M. High-temperature phase change materials for thermal energy storage. *Renewable and Sustainable Energy Reviews* **14**, 955-970, doi:10.1016/j.rser.2009.11.011 (2010).
- 13 Mohamed, S. A. *et al.* A review on current status and challenges of inorganic phase change materials for thermal energy storage systems. *Renewable and Sustainable Energy Reviews* **70**, 1072-1089, doi:10.1016/j.rser.2016.12.012 (2017).
- 14 Blanco-Rodríguez, P., Rodríguez-Aseguinolaza, J., Risueño, E. & Tello, M. Thermophysical

- characterization of Mg–51%Zn eutectic metal alloy: A phase change material for thermal energy storage in direct steam generation applications. *Energy* **72**, 414-420, doi:10.1016/j.energy.2014.05.058 (2014).
- 15 Risueño, E. *et al.* Mg-Zn-Al Eutectic Alloys as Phase Change Material for Latent Heat Thermal Energy Storage. *Energy Procedia* **69**, 1006-1013, doi:10.1016/j.egypro.2015.03.193 (2015).
- 16 Huang, X., Zhu, C., Lin, Y. & Fang, G. Thermal properties and applications of microencapsulated PCM for thermal energy storage: A review. *Appl. Therm. Eng.* **147**, 841-855, doi:10.1016/j.applthermaleng.2018.11.007 (2019).
- 17 Nomura, T., Zhu, C., Sheng, N., Saito, G. & Akiyama, T. Microencapsulation of Metal-based Phase Change Material for High-temperature Thermal Energy Storage. *Sci Rep-Uk* **5**, doi:doi.org/10.1038/srep09117 (2015).
- 18 Nomura, T. *et al.* Microencapsulated phase change materials with high heat capacity and high cyclic durability for high-temperature thermal energy storage and transportation. *Applied Energy* **188**, 9-18, doi:10.1016/j.apenergy.2016.11.025 (2017).
- 19 Sheng, N. *et al.* Development of a microencapsulated Al–Si phase change material with high-temperature thermal stability and durability over 3000 cycles. *Journal of Materials Chemistry A* **6**, 18143-18153, doi:10.1039/c8ta04708a (2018).
- 20 Desai, A. N., Gunjal, A. & Singh, V. K. Numerical investigations of fin efficacy for phase change material (PCM) based thermal control module. *Int. J. Heat Mass Transfer* **147**, doi:10.1016/j.ijheatmasstransfer.2019.118855 (2020).
- 21 Gokon, N., Nakamura, S., Hatamachi, T. & Kodama, T. Steam reforming of methane using double-walled reformer tubes containing high-temperature thermal storage Na₂CO₃/MgO composites for solar fuel production. *Energy* **68**, 773-782, doi:10.1016/j.energy.2014.01.107 (2014).
- 22 Pattison, R. C. & Baldea, M. A thermal-flywheel approach to distributed temperature control in microchannel reactors. *AIChE J.* **59**, 2051-2061, doi:10.1002/aic.13991 (2013).
- 23 Li, K. *et al.* A yolk/shell strategy for designing hybrid phase change materials for heat management in catalytic reactions. *Journal of Materials Chemistry A* **5**, 24232-24246, doi:10.1039/c7ta07147g (2017).
- 24 Aika, K. *et al.* Syntax of referencing in *Catalytic Handbook [Translated from Japanese.]* (ed. Catalysis society of Japan) 319-338 (Kodansha Ltd., 2008).
- 25 Tsuboi, Y., Takafuji, M., Ohara, H., Shinomiya, H., Takano, H., Izumiya, K. SNG Production from Woody Biomass Using Gasification Process. *Journal of the Combustion Society of Japan* **58**, 137-144, doi:DOI 10.20619/jcombsj.58.185_137 (2016).
- 26 Rönsch, S. *et al.* Review on methanation – From fundamentals to current projects. *Fuel*

- 166, 276-296, doi:10.1016/j.fuel.2015.10.111 (2016).
- 27 Falbo, L. *et al.* Kinetics of CO₂ methanation on a Ru-based catalyst at process conditions relevant for Power-to-Gas applications. *Applied Catalysis B: Environmental* **225**, 354-363, doi:10.1016/j.apcatb.2017.11.066 (2018).
- 28 Frontera, P., Macario, A., Ferraro, M. & Antonucci, P. Supported Catalysts for CO₂ Methanation: A Review. *Catalysts* **7**, doi:10.3390/catal7020059 (2017).
- 29 Meylan, F. D., Piguet, F.-P. & Erkman, S. Power-to-gas through CO₂ methanation: Assessment of the carbon balance regarding EU directives. *Journal of Energy Storage* **11**, 16-24, doi:10.1016/j.est.2016.12.005 (2017).
- 30 Götz, M. *et al.* Renewable Power-to-Gas: A technological and economic review. *Renewable Energy* **85**, 1371-1390, doi:10.1016/j.renene.2015.07.066 (2016).
- 31 Rahmani, S., Rezaei, M. & Meshkani, F. Preparation of highly active nickel catalysts supported on mesoporous nanocrystalline γ -Al₂O₃ for CO₂ methanation. *Journal of Industrial and Engineering Chemistry* **20**, 1346-1352, doi:10.1016/j.jiec.2013.07.017 (2014).
- 32 Lefebvre, J., Bajohr, S. & Kolb, T. Modeling of the transient behavior of a slurry bubble column reactor for CO₂ methanation, and comparison with a tube bundle reactor. *Renewable Energy* **151**, 118-136, doi:10.1016/j.renene.2019.11.008 (2020).
- 33 Try, R., Bengaouer, A., Baurens, P. & Jallut, C. Dynamic modeling and simulations of the behavior of a fixed-bed reactor-exchanger used for CO₂ methanation. *AIChE J.* **64**, 468-480, doi:10.1002/aic.15874 (2018).
- 34 Frey, M., Romero, T., Roger, A.-C. & Edouard, D. An intensification of the CO₂ methanation reaction: Effect of carbon nanofiber network on the hydrodynamic, thermal and catalytic properties of reactors filled with open cell foams. *Chem. Eng. Sci.* **195**, 271-280, doi:10.1016/j.ces.2018.11.028 (2019).
- 35 Sakamoto, K. Alumina Hydrate and Alumina [Translated from Japanese.]. *Journal of the japan institute of light metals* **22**, 295-308 (1972).
- 36 Garbarino, G., Riani, P., Magistri, L. & Busca, G. A study of the methanation of carbon dioxide on Ni/Al₂O₃ catalysts at atmospheric pressure. *Int. J. Hydrogen Energy* **39**, 11557-11565, doi:10.1016/j.ijhydene.2014.05.111 (2014).
- 37 Chein, R.-Y. & Wang, C.-C. Experimental Study on CO₂ Methanation over Ni/Al₂O₃, Ru/Al₂O₃, and Ru-Ni/Al₂O₃ Catalysts. *Catalysts* **10**, doi:10.3390/catal10101112 (2020).
- 38 Stangeland, K., Kalai, D., Li, H. & Yu, Z. CO₂ Methanation: The Effect of Catalysts and Reaction Conditions. *Energy Procedia* **105**, 2022-2027, doi:10.1016/j.egypro.2017.03.577 (2017).
- 39 Fujita, S. Mechanism of hydrogenation of carbon dioxide over metal catalysts [Translated from Japanese.]. *Doctoral dissertation in Hokkaido University*, doi:10.11501/3083386

- (1995).
- 40 Iwai, Y. Syntax of referencing in *Technology for practical application of heat storage systems and materials [Translated from Japanese.]* 137-145 (S & T publisher, 2018).
- 41 Zamengo, M., Ryu, J. & Kato, Y. Chemical Heat Storage of Thermal Energy from a Nuclear Reactor by Using a Magnesium Hydroxide/Expanded Graphite Composite Material. *Energy Procedia* **71**, 293-305, doi:10.1016/j.egypro.2014.11.882 (2015).
- 42 Shkatulov, A., Takasu, H., Kato, Y. & Aristov, Y. Thermochemical energy storage by LiNO₃-doped Mg(OH)₂: Rehydration study. *Journal of Energy Storage* **22**, 302-310, doi:10.1016/j.est.2019.01.014 (2019).

Acknowledgements

The authors greatly appreciate the financial support from the JSPS KAKENHI Grant Number 19K22224, 26th The thermal & Electric Energy Technology Inc. Foundation, and Steel Foundation for Environmental Protection Technology, Japan. A part of this work was conducted at Hokkaido University, supported by "Nanotechnology Platform" Program of the Ministry of Education, Culture, Sports, Science and Technology (MEXT), Japan.

Author contributions

T. T. conducted experiments, and wrote the manuscript. H. K., S. H., D. A., K. A., and Y. K., helped with experimental work and data analysis, reviewed and commented on the manuscript. T. N. conceived the idea, wrote the manuscript, and supervised the project.

Additional information

Competing financial interests: The authors declare no competing financial interests.

Figures

Exothermic reaction with shell & tube reactor

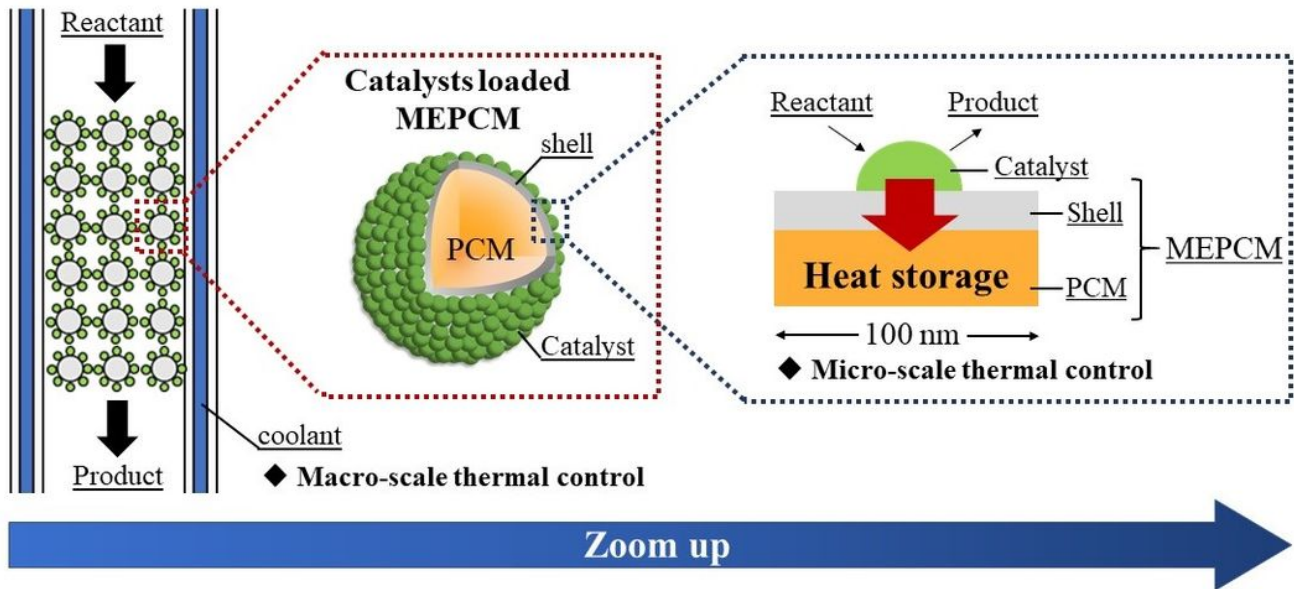


Figure 1

Schematic diagram of the catalyst-loaded MEPCM and the thermal control system.

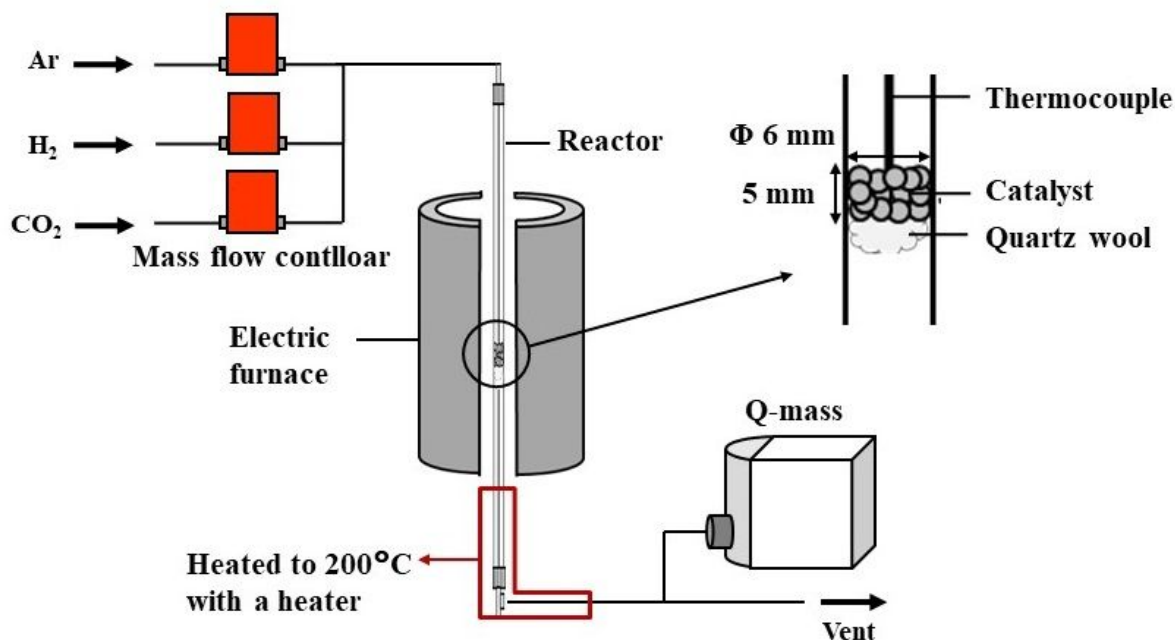


Figure 2

Schematic diagram of the vertical fixed bed tubular reactor.

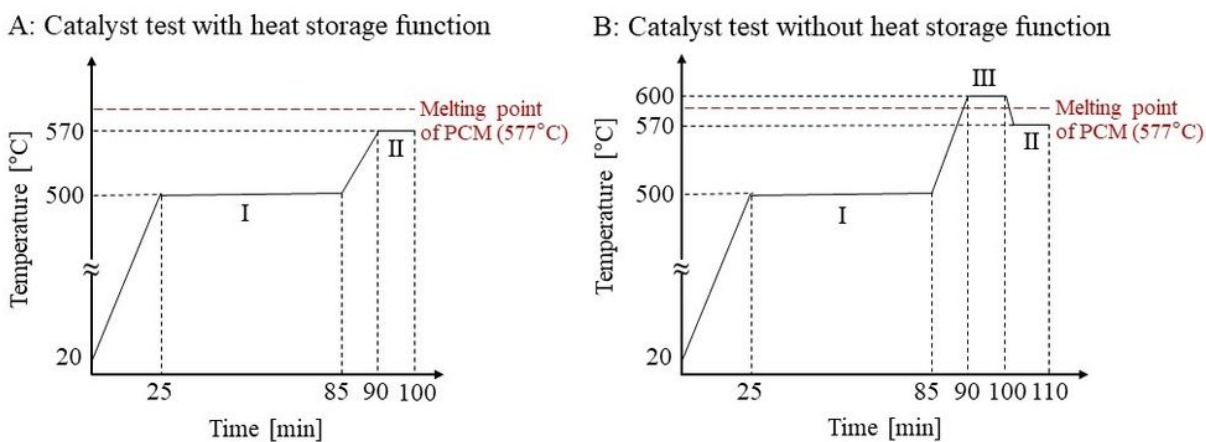


Figure 3

Temperature program of the two different reaction conditions. In the condition A, internal PCM is solid when reaction starts. In the condition B, internal PCM is liquid when reaction starts. Stage I: H₂ and Ar flow at 500 °C for the reduction of the sample. Stage II: Feed gas flow at 570 °C, and CO₂ methanation

reaction starts. Stage ②: Maintain at 600 °C for 10 minutes in Ar flow, which melt inside PCM to lose the heat storage capacity of the sample.

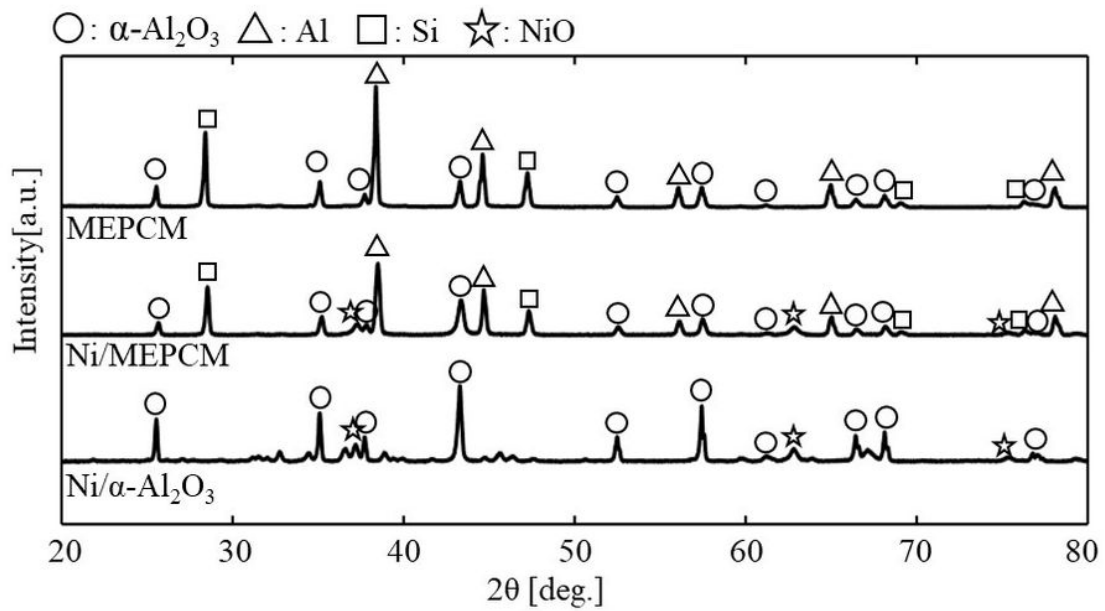


Figure 4

X-ray diffraction (XRD) patterns of the MEPCM, Ni/MEPCM, and Ni/ α -Al₂O₃.

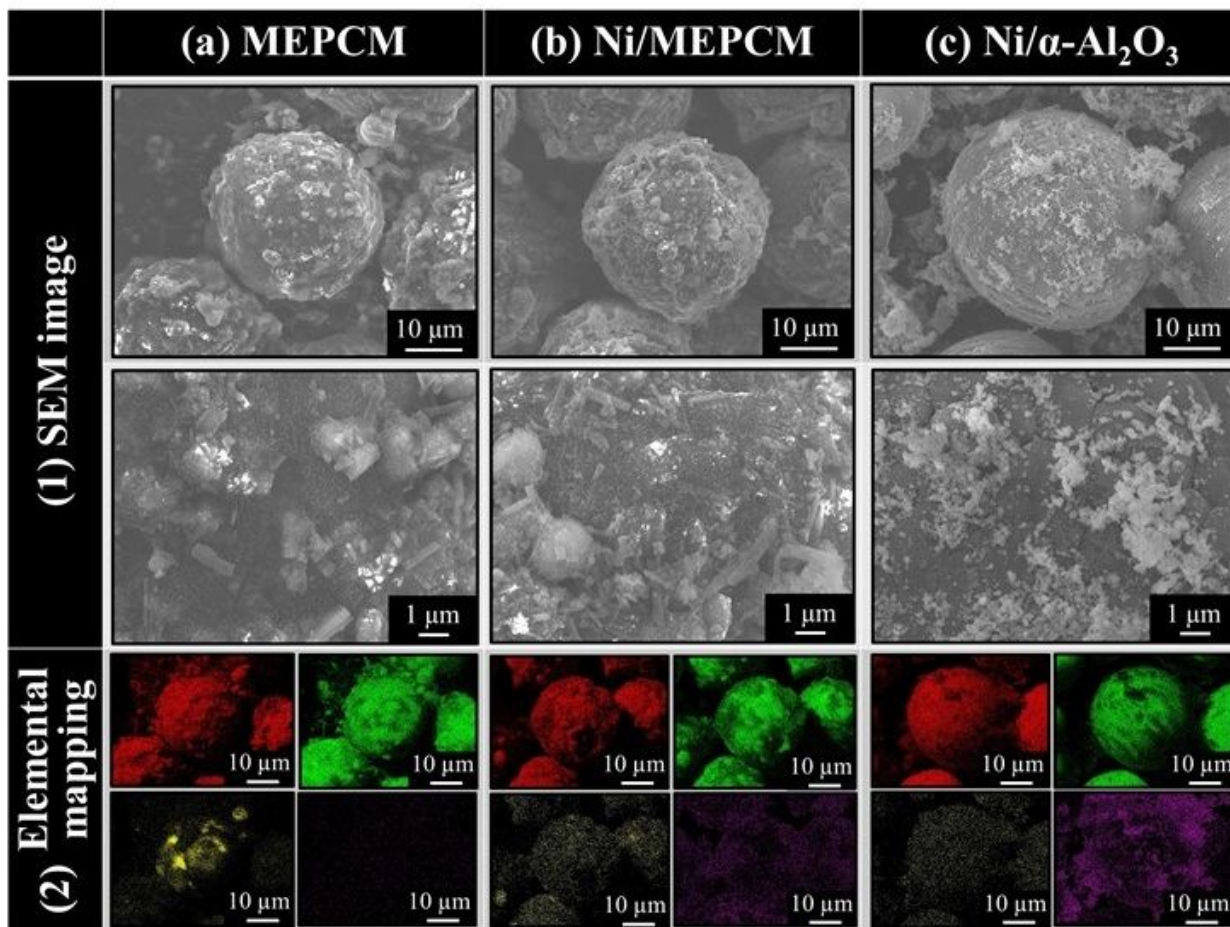


Figure 5

Scanning electron microscopy (SEM) image and the Energy dispersive spectroscopy (EDS) elemental mapping of the (a) MEPCM, (b) Ni/MEPCM, and (c) Ni/ α -Al₂O₃. In the elemental mapping, the red area represents O, the green area represents Al, the yellow area represents Si and the purple area represents Ni.

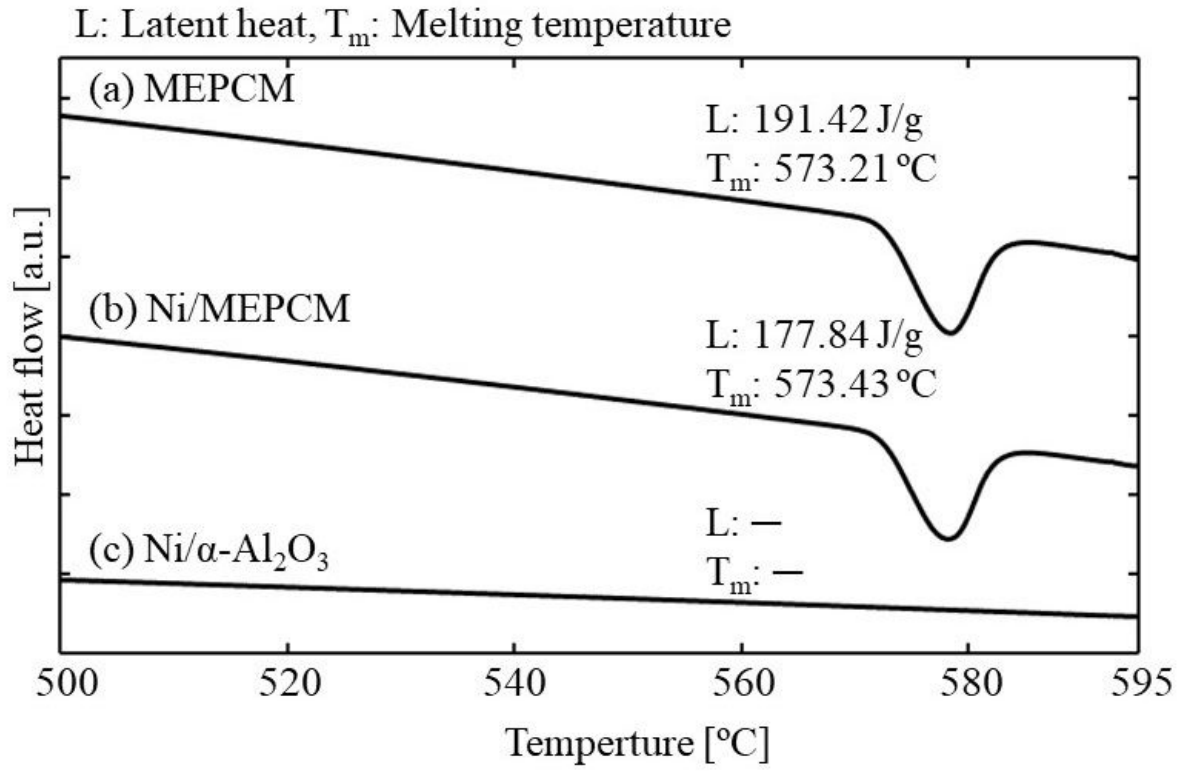


Figure 6

Heating DSC curves of the MEPCM, Ni/MEPCM, and Ni/ α -Al₂O₃.

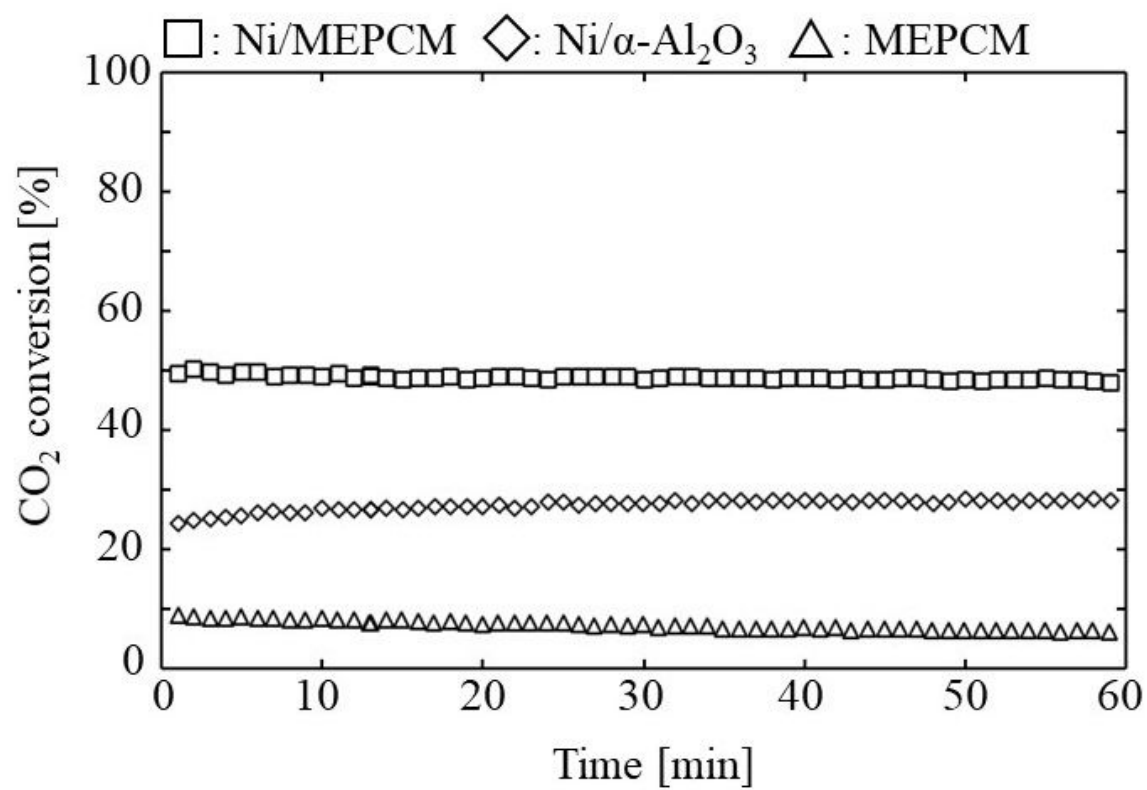


Figure 7

CO₂ conversion of the Ni/MEPCM, Ni/α-Al₂O₃, and MEPCM. Reaction condition: $\text{CO}_2 = 10 \text{ ml min}^{-1}$, $\text{H}_2 = 40 \text{ ml min}^{-1}$, $\text{N}_2 = 110 \text{ ml min}^{-1}$, Reaction temperature: 400°C.

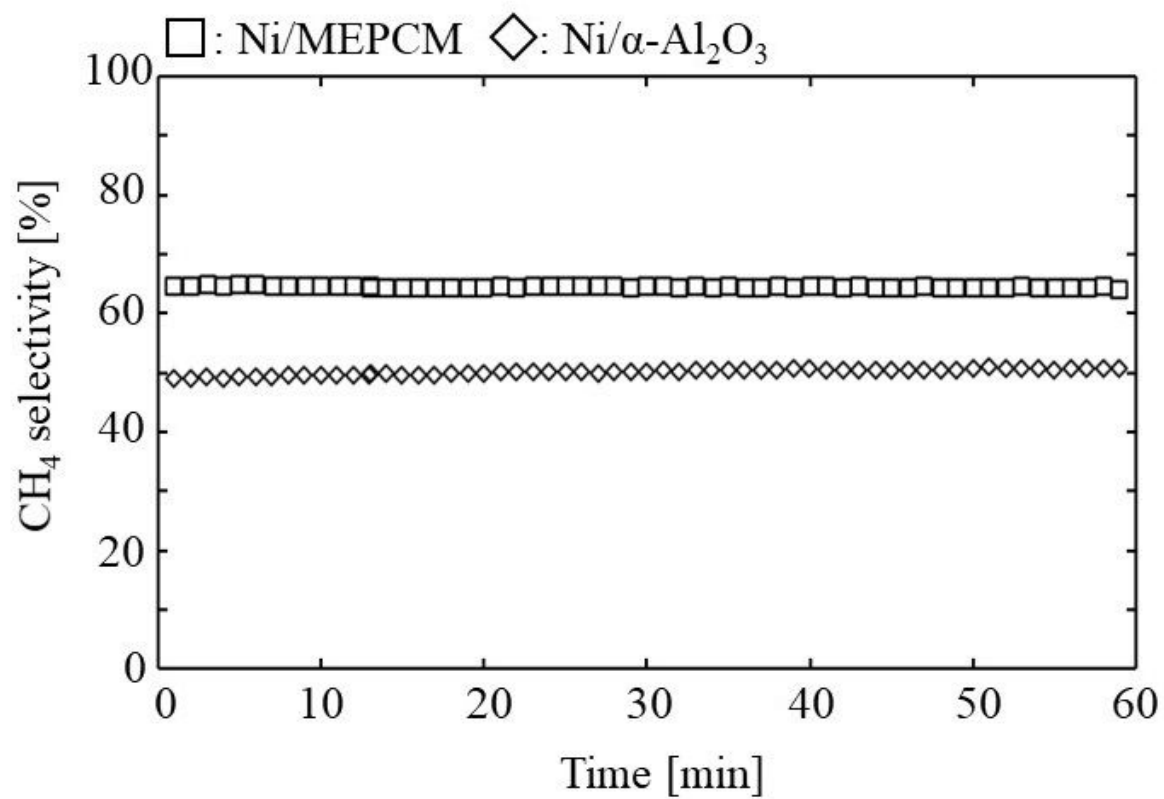


Figure 8

CH₄ selectivity of the Ni/MEPCM, Ni/α-Al₂O₃, and MEPCM. Reaction condition: CH₄,CO₂ = 10 ml min⁻¹, H₂, O₂ = 40 ml min⁻¹, N₂,Ar = 110 ml min⁻¹, Reaction temperature: 400°C.

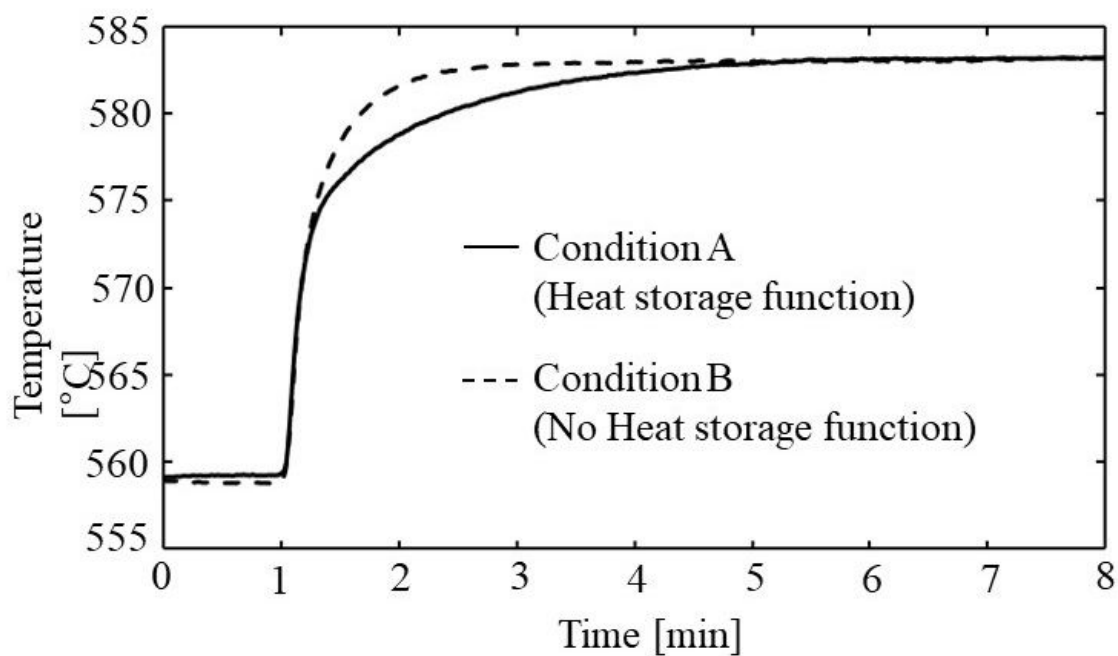


Figure 9

The temperature change of the Ni/MEPCM layer during CO₂ methanation. Feed gas was introduced at 1 min after the starts of measurement. In the condition A, the MEPCM has heat storage capacity. In the condition B, the MEPCM does not have it. Reaction condition: $\text{H}_2/\text{CO}_2 = 15 \text{ ml min}^{-1}$, $\text{H}_2/\text{N}_2 = 60 \text{ ml min}^{-1}$, $\text{H}_2/\text{Ar} = 50 \text{ ml min}^{-1}$, Reaction temperature: 570°C. Feed gas was introduced 1 min after the start of measurement.